LETTERS

Histone demethylase JHDM2A is critical for *Tnp1* and *Prm1* transcription and spermatogenesis

Yuki Okada[1,2], Greg Scott[3], Manas K. Ray[3], Yuji Mishina[3,4] & Yi Zhang[1,2]

Recent studies indicate that, similar to other covalent modifications, histone lysine methylation is subject to enzyme-catalysed reversion[1,2]. So far, LSD1 (also known as AOF2) and the jumonji C (JmjC)-domain-containing proteins have been shown to possess histone demethylase activity. LSD1 catalyses removal of H3K4me2/H3K4me1 through a flavin-adenine-dinucleotide-dependent oxidation reaction[3]. In contrast, JmjC-domain-containing proteins remove methyl groups from histones through a hydroxylation reaction that requires α-ketoglutarate and Fe(II) as cofactors[4]. Although an increasing number of histone demethylases have been identified and biochemically characterized[1,2], their biological functions, particularly in the context of an animal model, are poorly characterized. Here we use a loss-of-function approach to demonstrate that the mouse H3K9me2/1-specific demethylase JHDM2A (JmjC-domain-containing histone demethylase 2A, also known as JMJD1A) is essential for spermatogenesis. We show that *Jhdm2a*-deficient mice exhibit post-meiotic chromatin condensation defects, and that JHDM2A directly binds to and controls the expression of transition nuclear protein 1 (*Tnp1*) and protamine 1 (*Prm1*) genes, the products of which are required for packaging and condensation of sperm chromatin. Thus, our work uncovers a role for JHDM2A in spermatogenesis and reveals transition nuclear protein and protamine genes as direct targets of JHDM2A.

We have previously demonstrated that the histone demethylase JHDM2A has an important role in transcriptional activation mediated by the androgen receptor[5]. To further explore the biological function of this protein, we examined its expression pattern in mice. Similar to a previous report[6], we found that *Jhdm2a* is highly expressed in testis at both the messenger RNA and protein levels (data not shown). Further analysis of *Jhdm2a* by polymerase chain reaction with reverse transcription (RT–PCR) indicated that *Jhdm2a* levels (Fig. 1a, filled bars) increased significantly during spermatogenesis (~70-fold increase from day 7 testis to day 30 testis). In contrast, the level of the highly related gene *Jhdm2b* (also known as *Jmjd1b*) only varied 0.5–2.5-fold during spermatogenesis (Fig. 1a, open bars). When compared with several spermatogenesis marker genes (namely, zinc-finger- and BTB-domain-containing 16 (*Plzf*, also known as *Zbtb16*), synaptonemal complex protein 2 (*Sycp2*), transition nuclear protein 1 (*Tnp1*) and protamine 2 (*Prm2*)), *Jhdm2a* seems to be expressed during and after meiosis, preceding the expression of transition proteins and protamines (Fig. 1a, bottom panels). Western blot analysis using protein extracts of partially purified spermatocytes, round spermatids and elongating spermatids indicated that the level of JHDM2A is at the highest in round spermatids (Fig. 1b). Immunostaining revealed that JHDM2A protein is expressed in various spermatogenic stages of seminiferous tubules (Supplementary Fig. 1a), particularly in the nuclei of round spermatids (Fig. 1c, d), as well as in the nuclei and cytoplasm of Sertoli cells (Fig. 1c, arrowheads). Notably, JHDM2A protein was not detectable in spermatogonia or γ-H2AX-positive (also known as γ-H2AFX-positive) early pachytene spermatocytes (Fig. 1c, d arrows). A detailed analysis indicated that JHDM2A protein starts to be detected in the late pachytene stage, increases in diplotene and secondary spermatocytes, and reaches its highest level in round spermatids (Supplementary Fig. 1b, c). Interestingly, JHDM2A co-localizes with RNA polymerase II (phospho-Ser 5) in round spermatids as nuclear dots (Fig. 1e), and is excluded from the chromocentre and perinuclear heterochromatin (Fig. 1d, inset); this is consistent with the notion that JHDM2A functions as a transcriptional co-activator[5]. When spermatids start to elongate, JHDM2A localizes to the cytoplasm and forms distinct foci, which persist until spermiogenic step 13 and disappear in mature spermatozoa (Fig. 1f and Supplementary Fig. 1c).

The dynamic nature of JHDM2A expression during spermiogenesis indicates that it may have an important role in the late stages of male-germ-cell development. To explore this possibility, the mouse *Jhdm2a* gene was disrupted by insertion of a β-galactosidase/neomycin (*β-Geo*) cassette in intron 10 (or intron 7 of splicing variant 2) (Fig. 2a and Supplementary Fig. 2a). Chimaeras and heterozygous ($Jhdm2a^{+/G}$) mice were obtained using standard procedures. Homozygous mice that carry the *β-Geo* alleles ($Jhdm2a^{G/G}$) were obtained by crossing heterozygous pairs. Homozygous mice, verified by Southern blot analysis (Supplementary Fig. 2b, c), were viable and were born at mendelian ratios (data not shown). Expression of the *Jhdm2a*(exon 1–10)–*β-Geo* fusion transcript was confirmed by RT–PCR in $Jhdm2a^{+/G}$ and $Jhdm2a^{G/G}$ mice (Fig. 2b, bottom panel). However, a low level (~10%) of wild-type mRNA was also detected in $Jhdm2a^{G/G}$ mice (Fig. 2b, top panel, lane 5, and Fig. 2c).

The *Jhdm2a* mutant allele encodes the first 506 amino acids of JHDM2A and is fused to β-GEO (Fig. 2d). Given that the catalytic JmjC domain is deleted, the mutant protein will not be enzymatically active. Whole-mount β-Gal staining confirmed the expression of the β-Gal protein in testis in a dose-dependent manner (Fig. 2e). Western blot analysis demonstrated that the JHDM2A protein in the testis was detected as a doublet, which corresponds to the full-length (V1, 152 kilodaltons (kDa)) and the splicing variant (V2, 139 kDa) (Fig. 2f, top panel, and Supplementary Fig. 2a). Although the splicing variant was not detectable, lower levels of full-length JHDM2A protein still remain in the $Jhdm2a^{G/G}$ mice (Fig. 2f, top panel). As expected, the JHDM2A(1–506)–β-Gal fusion protein was produced in both $Jhdm2a^{+/G}$ and $Jhdm2a^{G/G}$ mice (Fig. 2f, second panel), and this fusion protein was also detectable by an anti-JHDM2A antibody (data not shown). Neither JHDM2B, a related H3K9 demethylase[5], nor DNMT3B, a *de novo* DNA methyltransferase expressed in early meiosis and round spermatids[7], was affected by *Jhdm2a* disruption (Fig. 2f).

[1]Howard Hughes Medical Institute, [2]Department of Biochemistry and Biophysics, Lineberger Comprehensive Cancer Center, University of North Carolina at Chapel Hill, Chapel Hill, North Carolina 27599-7295, USA. [3]The Knock Out Core, [4]Molecular Developmental Biology Group, Laboratory of Reproductive and Developmental Toxicology, National Institutes of Health, Research Triangle Park, North Carolina 27709, USA.

Consistent with having smaller testes (Fig. 2e and Supplementary Table 1) and a significantly lower sperm count (Supplementary Table 1), *Jhdm2a*$^{G/G}$ male mice were infertile (data not shown). Histological analysis revealed multiple vacuolations in seminiferous tubules and fewer elongated spermatids in *Jhdm2a*$^{G/G}$ testis (Supplementary Fig. 3a). A detailed examination revealed that noticeable morphological defects start from the spermiogenic stage-XI–XII spermatids having less-elongated heads (Fig. 3a, inset). Spermatids in *Jhdm2a*$^{G/G}$ mice remain unelongated at stage I and II–III (Fig. 3a, insets); the number of spermatids greatly decreased and the spermatids are not properly elongated at stage IV–VIII (Fig. 3a). At stage VIII, multiple spermatids sharing their cytoplasms and having multiple tails are observed (Fig. 3a, stage VIII, arrow). Electron microscopic analysis revealed abnormal nuclear structure including loss of chromocentre organization (Fig. 3b, step 2–3) and loss of polarity of chromatin distribution (Fig. 3b, steps 7 and 9). Although the acrosomal structure in round spermatids seems to be normal at step 7, it is not fully formed in step 13 (Fig. 3b). In contrast to the multiple post-meiotic defects, pre-meiotic germ cells, Sertoli cells and Leydig cells are morphologically normal (Supplementary Fig. 3a, b). Thus, the main function of JHDM2A is in the post-meiotic stage of spermatogenesis.

In agreement with the defects described above, few mature sperm were observed in the epididymis of *Jhdm2a*$^{G/G}$ mice (Supplementary Fig. 3c). Of the few sperm recovered from the epididymis of the mutant mice, all have abnormally shaped heads (Fig. 3c). Although the mutant sperm have tails, 98.5% of them are immotile (Fig. 3d). To assess the packaging state of the sperm DNA, we performed acridine orange staining, an assay that can distinguish the packaging state of the sperm DNA on the basis of whether the sperm are fluorescent green only or both green and red[8]. The fact that the abnormal sperm heads from *Jhdm2a*$^{G/G}$ stained both green and red by acridine orange (Fig. 3e) indicates that the sperm heads from mutant mice are defective in chromatin condensation. Flow cytometry analysis also revealed that sperm from *Jhdm2a*$^{G/G}$ mice have a DNA content that peaks between round and condensed spermatids (Supplementary Fig. 3d), consistent with defects in chromatin condensation[9]. Collectively, the above results support the idea that incomplete chromatin condensation is the cause of the infertility of male *Jhdm2a*$^{G/G}$ mice.

Mice lacking the H3K9 methyltransferases SUV39H1 and SUV39H2 have meiotic defects[10], indicating that maintaining an appropriate H3K9 methylation level is important for meiosis during spermatogenesis. To evaluate whether loss of *Jhdm2a* function affects

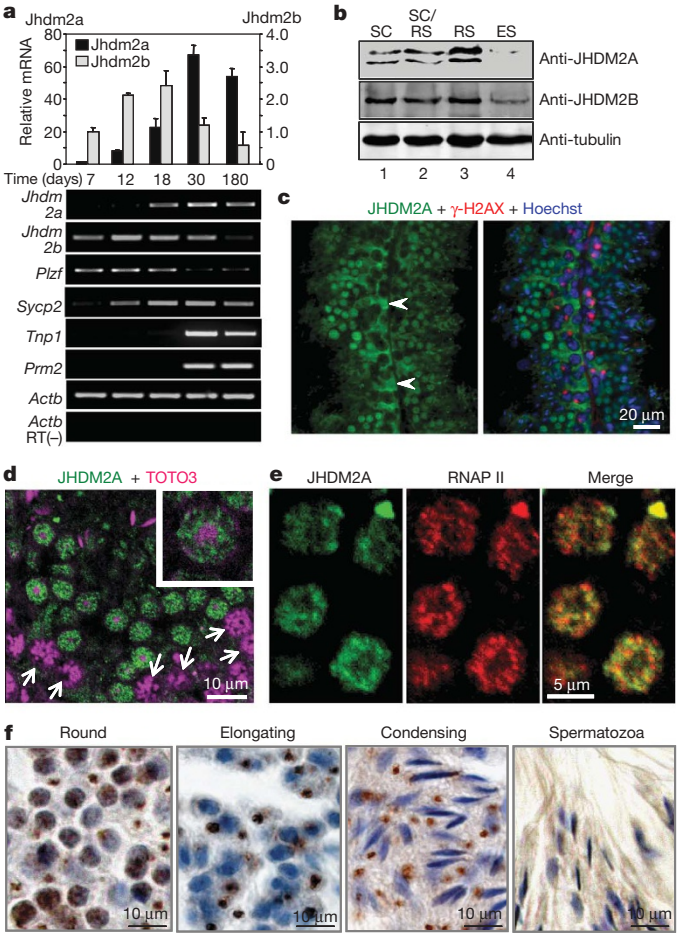

Figure 1 | *Jhdm2a* expression is largely restricted to post-meiotic male germ cells. **a**, Top panel, quantitative RT–PCR analysis of the *Jhdm2a* and *Jhdm2b* expression levels in testis from mice of different ages. The expression level in day 7 mouse testis was arbitrarily set as 1. Data presented are means ± s.d. from three independent experiments. Lower panels are RT–PCR results of various genes in testes of different developmental stages. *Plzf*, spermatogonia-specific; *Sycp2*, spermatocyte-specific; *Tnp1*, post-meiosis-specific; and *Prm2*, post-meiosis-specific. *Actb* (β-actin) serves as a control. RT–, reverse transcriptase minus. **b**, Western blot analysis of JHDM2A and JHDM2B expression. ES, elongating spermatid; RS, round spermatid; and SC, spermatocyte. Lane 1, SCs with ~30% RS contamination. Lane 2, SCs and RSs (~50% each). Lane 3, RSs with ~30% SC contamination. Lane 4, mouse ES cells. Tubulin serves as a loading control. **c**, Expression of JHDM2A in seminiferous tubules. JHDM2A (green), γ-H2AX (red) and Hoechst (DNA, blue). Arrowheads, Sertoli cells. **d**, Confocal microscopic analysis of JHDM2A in stage V seminiferous tubules. JHDM2A (green) and TOTO3 (DNA, magenta). Arrows, pacytene spermatocytes. **e**, Co-localization of JHDM2A (green) and RNA polymerase II (RNAP II, red) in round spermatids. **f**, Dynamic expression pattern of JHDM2A in various stages of post-meiotic male germ cells. Immunopositive cells are stained brown. Counterstaining by haematoxylin is blue.

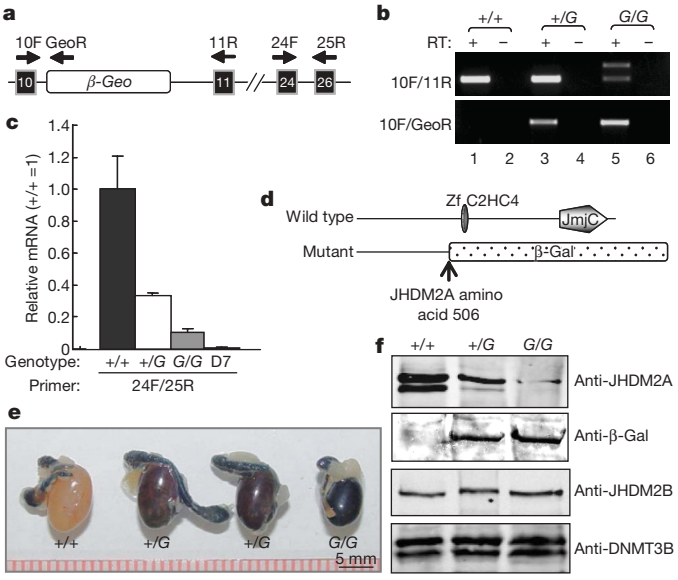

Figure 2 | *Jhdm2a* mutant mice are hypomorphic. **a**, Diagram of the *Jhdm2a* mutant allele derived from clone YHA186 (BayGenomics). Arrows, primers used in **b** and **c**. Black boxes with numbers refer to the respective exons of the *Jhdm2a* gene. **b**, RT–PCR analysis of the expression of the wild-type and mutant alleles in *Jhdm2a*$^{+/+}$, *Jhdm2a*$^{+/G}$ and *Jhdm2a*$^{G/G}$ mouse testis. Total RNA isolated from testis was used for RT–PCR. **c**, Quantitative RT–PCR analysis of the expression of the 3′ end of *Jhdm2a*. D7, total RNA isolated from wild-type day 7 mouse testis. The expression level in adult *Jhdm2a*$^{+/+}$ is arbitrarily defined as 1. Data presented are means ± s.d. from three mice for each genotype. **d**, Diagram of the wild-type and mutant protein alleles. The mutant allele creates a fusion protein of JHDM2A(1–506)–β-Gal. Zf C2HC4, C2HC4 type zinc finger motif. **e**, Whole-mount β-galactosidase staining in testes of indicated genotypes. **f**, Western blot analysis of JHDM2A and JHDM2A(1–506)–β-Gal fusion protein expression in testis of indicated genotypes. Equal amounts of total testis nuclear extracts were used in the blot. The antibodies used are indicated.

global H3K9 methylation levels during spermatogenesis, we performed immunostaining. In contrast to a previous report[11], we found that both H3K9me2 and H3K9me3 levels were relatively low in spermatocytes, and were high in spermatogonia and spermatids in wild-type testis (Supplementary Fig. 4a, b). This methylation pattern is maintained in the *Jhdm2a*$^{G/G}$ seminiferous tubules (Supplementary Fig. 4a, b). However, the H3K9me3 staining pattern in round spermatids became more diffuse in the mutant compared to in the wild-type testis (Supplementary Fig. 4d), although no significant change in the total H3K9 methylation levels was detected (Supplementary Fig. 4e). The decreased H4 acetylation level was probably due to a decreased number of elongating/condensing spermatids in the mutant testis (Supplementary Fig. 4c, e)[12]. Because active DNA demethylation has been reported in spermatocytes[13], and there is a tight correlation between DNA methylation and H3K9 methylation during germ-cell development[14], we analysed the effect of loss of *Jhdm2a* function on DNA methylation in seminiferous tubules. Results shown in Supplementary Fig. 5 revealed no significant differences. Therefore, loss of *Jhdm2a* function does not have global effect on H3K9 or DNA methylation in testis.

Multiple molecular events have to occur for a round spermatid to become a mature sperm. These events include chromatin condensation, reorganization of the spermatid nucleus, formation of an acrosome and assembly of a sperm tail[15]. To accomplish these events, a number of postmeiotic proteins including transition nuclear proteins, protamines and testis-specific histone variants, such as H1T (also known as histone cluster H1T, HISTH1T), H1T2 (also known as histone family member N, testis specific, H1FNT) and HILS1 (histone linker H1 domain, spermatid-specific 1), have to be synthesized properly. Consequently, mice that lack the proteins mentioned above display impaired spermiogenesis and male infertility[16]. Defective chromatin condensation similar to that observed in the *Jhdm2a*$^{G/G}$ mice was reported in the knockout mice for transition nuclear proteins, protamines, H1T2 and TLP (TBP-like protein, also known as TBPL1), raising the possibility that *Jhdm2a* may contribute to spermiogenesis by regulating expression of some of these genes[17–20]. To explore this possibility, we attempted to purify round spermatids, in which JHDM2A is highly expressed, from *Jhdm2a*$^{+/+}$ and *Jhdm2a*$^{G/G}$ testes. Purity of the isolated cells was confirmed by examining the expression profile of stage-specific genes (Supplementary Fig. 6). Quantitative (q)RT–PCR demonstrated that, although the expression of most genes tested was not significantly altered, the expression of *Tnp1* and *Prm1* was significantly reduced in the *Jhdm2a*$^{G/G}$ round spermatids (Fig. 4a).

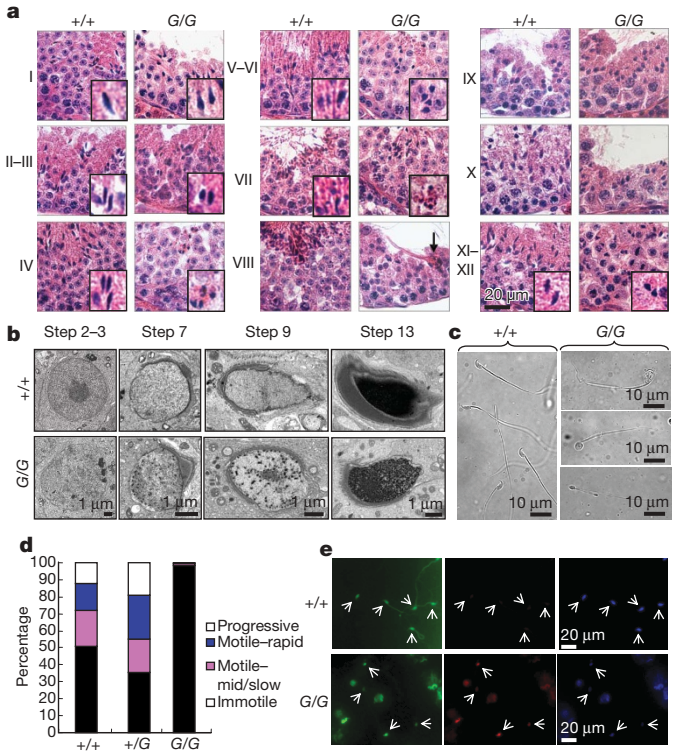

Figure 3 | Defective chromatin condensation in *Jhdm2a*$^{G/G}$ spermatids. **a**, Haematoxylin and eosin staining shows the histopathological features of testis from seven-month-old *Jhdm2a*$^{+/+}$ (+/+) and *Jhdm2a*$^{G/G}$ (*G*/*G*) mice. Roman numerals refer to the stages of mouse spermatogenesis. In *Jhdm2a*$^{G/G}$ mouse testis, spermatids with abnormal elongation were initially observed at stage XI (step 11). Insets represent higher-magnification images of elongated spermatids. **b**, Electron microscopy analysis of *Jhdm2a*$^{+/+}$ (+/+) and *Jhdm2a*$^{G/G}$ (*G*/*G*) spermatids. Chromocentre at step 2–3 of *Jhdm2a*$^{G/G}$ spermatids is indistinct. In steps 7–9, heterochromatin distribution loses polarity. In step 13, chromatin condensation is defective. **c**, Abnormal morphology of spermatozoa isolated from cauda epididymis of *Jhdm2a*$^{G/G}$ (*G*/*G*) compared to spermatozoa from *Jhdm2a*$^{+/+}$ (+/+). *Jhdm2a*$^{G/G}$ spermatozoa exhibit round shaped heads and variable size. **d**, Sperm motility analysis of the indicated genotypes. **e**, Acridine orange staining of spermatozoa from *Jhdm2a*$^{+/+}$ (+/+) and *Jhdm2a*$^{G/G}$ (*G*/*G*) mice. Spermatozoa with complete chromatin condensation are only stained green, but are stained both green and red if their chromatin condensation is incomplete. Arrows indicate individual sperm. Blue staining represents Hoechst.

Chromatin immunoprecipitation (ChIP) analysis using testicular cells demonstrated that JHDM2A was specifically recruited to region C of the *Prm1* gene (Fig. 4b, compare lanes 3 and 6). Although the JHDM2A(1–506)–β-Gal fusion protein can be recognized by our anti-JHDM2A antibody, the fusion protein does not occupy the *Prm1* promoter, suggesting the deleted carboxy-terminal region of JHDM2A is required for chromatin association. ChIP–qPCR analysis using purified round spermatids confirmed specific enrichment of JHDM2A to the core promoter of the *Prm1* gene (Fig. 4c). Similar results were obtained for the *Tnp1* gene, but not the *Tnp2* gene (Fig. 4c), consistent with its specific effects on *Prm1* and *Tnp1* gene expression (Fig. 4a). To evaluate the effect of JHDM2A binding on H3K9 methylation, we compared the H3K9 methylation levels of *Prm1* and *Tnp1* in *Jhdm2a*$^{+/+}$ and *Jhdm2a*$^{G/G}$ round spermatids. Results shown in Fig. 4d demonstrate that H3K9 methylation levels were significantly increased in the promoter regions of both genes in *Jhdm2a*$^{G/G}$ spermatids relative to that in *Jhdm2a*$^{+/+}$ spermatids. However, the changes of H3K9 methylation levels were much less pronounced in a region ~1 kb upstream of the transcription start site (5′) of the corresponding genes (Fig. 4d). Interestingly, a significant increase in the H3K9me3 level at both gene promoters is observed in the *Jhdm2a*$^{G/G}$ spermatids, despite previous demonstration that JHDM2A is incapable of removal of H3K9me3 *in vitro*[5]. It is possible that JHDM2A may associate with a co-factor that confers its substrate specificity when bound to the two promoters. Collectively, the above results support the notion that JHDM2A directly contributes to the expression of *Tnp1* and *Prm1* genes by binding to and removing the silencing H3K9 methyl mark at their promoters.

Through a loss-of-function approach, we demonstrated that *Jhdm2a* is indispensable for spermiogenesis. This function is consistent with its unique expression pattern in round and elongating spermatids. Our studies suggest that JHDM2A participates in spermiogenesis by regulating the expression of specific target genes such as *Tnp1* and *Prm1*, which are required for histone replacement during the final stages of sperm chromatin condensation and maturation (Supplementary Fig. 7). It is important to point out that, although residual amounts of the wild-type JHDM2A are still expressed in the *Jhdm2a*$^{G/G}$ mouse, and we cannot rule out the possibility that the phenotype might be the result of a dominant negative from the JHDM2A–β-Gal fusion protein, we observed the same phenotype in mice with a *Jhdm2a* allele that disrupts the JmjC domain, indicating that the *Jhdm2a*$^{G/G}$ allele phenocopies a true null (Y.O. and Y.Z., unpublished data. The fact that spermatogenesis is under the control of the hypothalamic–pituitary axis and is governed by hormones such as follicle-stimulating hormone and leutinizing hormone raises

questions of whether the spermiogenesis defects observed in the *Jhdm2a* mutant mice are a secondary effect of hormonal or physiological pathway alternations. This is unlikely to be the case because no significant alternations in hormone levels are detected in the mutant mice (Supplementary Fig. 8). Consistently, no obvious morphological defects in Leydig or Sertoli cells are observed (Supplementary Fig. 3b). Indeed, we have not observed any additional phenotypes for the *Jhdm2a*$^{G/G}$ mice, supporting the contention that a main function of JHDM2A is in spermatogenesis. Although there are several knockout mouse models that exhibit male infertility phenotypes similar to those observed in human syndromes such as azoospermia or globozoospermia[21], most of the genes disrupted in mice are intact in human patients, raising the possibility that *Jhdm2a* might be a new candidate gene involved in these infertility syndromes.

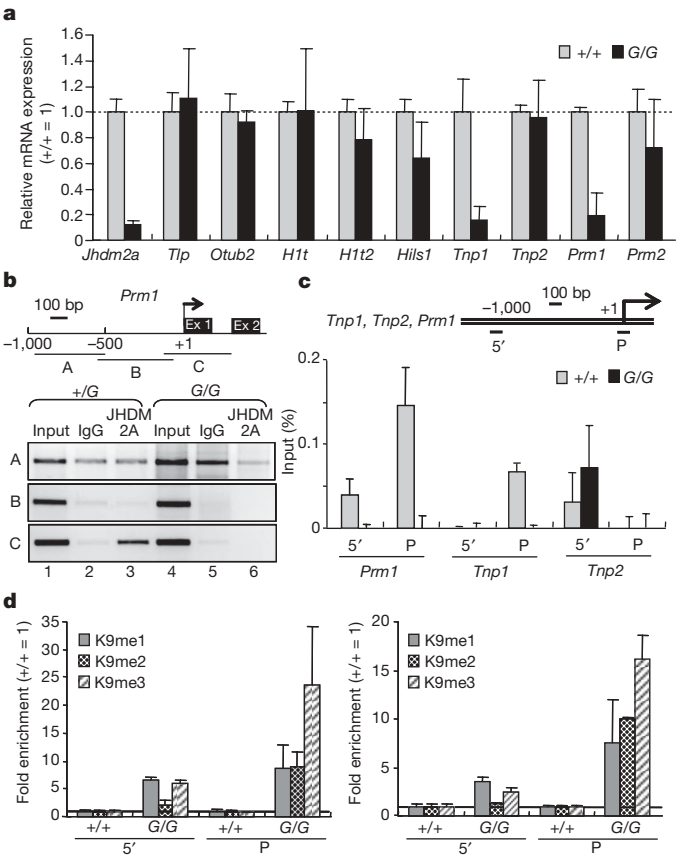

Figure 4 | JHDM2A positively regulates *Tnp1* and *Prm1* genes in round spermatids. a, Quantitative RT–PCR analysis of the expression levels of selected genes in round spermatids from mice of indicated genotypes. *Otub*, OTU domain, ubiquitin aldehyde binding 2. For *Jhdm2a*, primers 24F and 25R shown in Fig. 2a were used. Results were normalized to *Actb*, and the expression level in *Jhdm2a*$^{+/+}$ (+/+) is defined as 1. Data are presented as means ± s.d. from three or four independent experiments. **b**, Top panel, diagram of mouse *Prm1* gene structure. A region 1 kb upstream of the transcription start site and first exon is covered by three primer sets (A, −980–−486; B, −551–−55; C, −124–+326). Bottom panel, ChIP analysis indicates that JHDM2A is recruited to a region that overlaps with the transcriptional start site of the *Prm1* gene (region 'C'). Input, 0.25%; IgG, rabbit immunoglobulin G; JHDM2A, anti-JHDM2A antibody. **c**, Top panel, diagram of mouse *Tnp1*, *Tnp2* and *Prm1* genes, and location of primers used for ChIP-qPCR. Bottom panel, ChIP-qPCR analysis examining recruitment of JHDM2A to promoter (P) and 1 kb upstream of transcriptional start site (5′) of *Prm1*, *Tnp1* and *Tnp2* genes. The results were normalized to IgG control, and were shown as percentage of enrichment relative to input. Signals detected in the 5′ of Tnp2 are from non-specific PCR amplification. Data are presented as means ± s.d. from three independent experiments. **d**, Comparison of H3K9 methylation levels of JHDM2A-binding sites of *Prm1* and *Tnp1* genes in *Jhdm2a*$^{+/+}$ (+/+) and *Jhdm2a*$^{G/G}$ (*G*/*G*) round spermatids by ChIP-qPCR. K9me1, K9me2 and K9me3 indicate anti-monomethyl, -dimethyl and -trimethyl H3K9 antibody, respectively. Results were normalized to histone H3, and are shown as fold of enrichment compared to that in the wild type (+/+). Data are presented as means ± s.d. from three independent experiments.

METHODS SUMMARY

Generation of *Jhdm2a*$^{G/G}$ mice. An ES clone with *Jhdm2a* gene-trap allele (YHA186) was purchased from BayGenomics (http://baygenomics.ucsf.edu/). The ES cells were injected into C57BL/6 blastocysts using standard procedures. After confirmation of germ-line transmission, the progeny was backcrossed to C57BL/6 once, and the *Jhdm2a*$^{G/G}$ line was obtained by crossing heterozygous (*Jhdm2a*$^{+/G}$) mice.

Histology, immunostaining and β-galactosidase staining. For paraffin-embedded sections, dissected testes were fixed with either Bouin's fixative or 4% paraformaldehyde. For frozen sections, tissues were briefly fixed with 4% paraformaldehyde, dehydrated by sucrose, and embedded in optimal cutting temperature (OCT) compound (SAKURA). For non-fluorescent detection, an RTU vector staining kit was used (Vector laboratories). For β-galactosidase staining, tissues were fixed with 0.2% glutaraldehyde/2% formaldehyde buffer for 20 min. After rinsing with 0.1 M phosphate buffer (pH 7.3), they were stained with 1 mg ml^{-1} 5-bromo-4-chloro-3-indoyl-β-D-galactoside (X-gal), 5 mM potassium ferricyanide and 5 mM potassium ferrocyanide in rinsing buffer at 37 °C for 4 h to overnight.

RT–PCR and qRT–PCR. Total RNA was purified from testes using a RNeasy kit (Qiagen). After DNase I treatment, first-strand DNA synthesis was performed using Improm II (Promega). Ex Taq polymerase (TAKARA) and SYBR Green PCR master mix (Applied Biosystems) were used for PCR and qPCR, respectively. PCR conditions and primer sequences are listed in Supplementary Table 2.

ChIP and ChIP/qPCR. Spermatogenic cell fractionation was performed as described[22]. Cells recovered from each gradient fraction were partially stained by 4,6-diamidino-2-phenylindole (DAPI) to determine their purity. Selected fractions were pooled for specific developmental stages and their purity was further verified by RT–PCR using stage-specific marker genes (Supplementary Fig. 6). Cells (1×10^6 and 5×10^6) were used for ChIP analysis with modification-specific anti-histone antibodies and anti-JHDM2A antibodies as described previously[23]. Ex Taq polymerase and SYBR Green PCR master mix were used for PCR and qPCR, respectively. PCR conditions and primer sequences are listed in Supplementary Table 2.

Full Methods and any associated references are available in the online version of the paper at www.nature.com/nature.

Received 13 July; accepted 5 September 2007.
Published online 17 October 2007.

1. Klose, R. J. & Zhang, Y. Regulation of histone methylation by demethylimination and demethylation. *Nature Rev. Mol. Cell Biol.* **8**, 307–318 (2007).
2. Shi, Y. & Whetstine, J. R. Dynamic regulation of histone lysine methylation by demethylases. *Mol. Cell* **25**, 1–14 (2007).
3. Shi, Y. *et al.* Histone demethylation mediated by the nuclear amine oxidase homolog LSD1. *Cell* **119**, 941–953 (2004).
4. Tsukada, Y. *et al.* Histone demethylation by a family of JmjC domain-containing proteins. *Nature* **439**, 811–816 (2006).
5. Yamane, K. *et al.* JHDM2A, a JmjC-containing H3K9 demethylase, facilitates transcription activation by androgen receptor. *Cell* **125**, 483–495 (2006).
6. Hoog, C., Schalling, M., Grunder-Brundell, E. & Daneholt, B. Analysis of a murine male germ cell-specific transcript that encodes a putative zinc finger protein. *Mol. Reprod. Dev.* **30**, 173–181 (1991).
7. La Salle, S. & Trasler, J. M. Dynamic expression of DNMT3a and DNMT3b isoforms during male germ cell development in the mouse. *Dev. Biol.* **296**, 71–82 (2006).
8. Kosower, N. S., Katayose, H. & Yanagimachi, R. Thiol-disulfide status and acridine orange fluorescence of mammalian sperm nuclei. *J. Androl.* **13**, 342–348 (1992).
9. Traina, M. E. *et al.* Long-lasting effects of lindane on mouse spermatogenesis induced by *in utero* exposure. *Reprod. Toxicol.* **17**, 25–35 (2003).
10. Peters, A. H. *et al.* Loss of the Suv39h histone methyltransferases impairs mammalian heterochromatin and genome stability. *Cell* **107**, 323–337 (2001).
11. Payne, C. & Braun, R. E. Histone lysine trimethylation exhibits a distinct perinuclear distribution in Plzf-expressing spermatogonia. *Dev. Biol.* **293**, 461–472 (2006).
12. Meistrich, M. L., Trostle-Weige, P. K., Lin, R., Bhatnagar, Y. M. & Allis, C. D. Highly acetylated H4 is associated with histone displacement in rat spermatids. *Mol. Reprod. Dev.* **31**, 170–181 (1992).
13. Loukinov, D. I. *et al.* BORIS, a novel male germ-line-specific protein associated with epigenetic reprogramming events, shares the same 11-zinc-finger domain

with CTCF, the insulator protein involved in reading imprinting marks in the soma. *Proc. Natl Acad. Sci. USA* **99,** 6806–6811 (2002).
14. Seki, Y. *et al.* Extensive and orderly reprogramming of genome-wide chromatin modifications associated with specification and early development of germ cells in mice. *Dev. Biol.* **278,** 440–458 (2005).
15. Sassone-Corsi, P. Unique chromatin remodeling and transcriptional regulation in spermatogenesis. *Science* **296,** 2176–2178 (2002).
16. de Rooij, D. G. & de Boer, P. Specific arrests of spermatogenesis in genetically modified and mutant mice. *Cytogenet. Genome Res.* **103,** 267–276 (2003).
17. Cho, C. *et al.* Haploinsufficiency of protamine-1 or -2 causes infertility in mice. *Nature Genet.* **28,** 82–86 (2001).
18. Martianov, I. *et al.* Polar nuclear localization of H1T2, a histone H1 variant, required for spermatid elongation and DNA condensation during spermiogenesis. *Proc. Natl Acad. Sci. USA* **102,** 2808–2813 (2005).
19. Martianov, I. *et al.* Late arrest of spermiogenesis and germ cell apoptosis in mice lacking the TBP-like *TLF/TRF2* gene. *Mol. Cell* **7,** 509–515 (2001).
20. Zhao, M. *et al.* Transition nuclear proteins are required for normal chromatin condensation and functional sperm development. *Genesis* **38,** 200–213 (2004).
21. Matzuk, M. M. & Lamb, D. J. Genetic dissection of mammalian fertility pathways. *Nature Cell Biol.* **4** (Suppl), s41–s49 (2002).
22. Pivot-Pajot, C. *et al.* Acetylation-dependent chromatin reorganization by BRDT, a testis-specific bromodomain-containing protein. *Mol. Cell. Biol.* **23,** 5354–5365 (2003).
23. Okada, Y. *et al.* Leukaemic transformation by CALM-AF10 involves upregulation of Hoxa5 by hDOT1L. *Nature Cell Biol.* **8,** 1017–1024 (2006).

Supplementary Information is linked to the online version of the paper at www.nature.com/nature.

Acknowledgements We thank T. Ward, V. Madden, R. Bagnell Jr and K. Moore for technical assistance, and K. Yamane for anti-JHDM2B antibody. We are grateful to R. Klose, E. Kallin and K. Gardner for reading of the manuscript. This work was supported by the NIH (Y.Z.), and in part by the Intramural Research Program of the NIH, NIEHS (Y.M.). Y.Z. is an Investigator of the Howard Hughes Medical Institute.

Author Contributions Y.O. and Y.Z. designed the experiments and prepared the manuscript. Y.O. performed the experiments. G.S., M.K.R. and Y.M. generated the chimaera mice from the BayGenomics ES clone.

Author Information Reprints and permissions information is available at www.nature.com/reprints. Correspondence and requests for materials should be addressed to Y.Z. (yi_zhang@med.unc.edu).

METHODS

Generation of *Jhdm2a*$^{G/G}$ mice. All mouse experiments were performed in accordance with institute guidelines covering the humane care and use of animals in research. Genotyping was performed by Southern blotting using 2 μg of tail DNA digested with either *Eco*RV or *Sph*I as shown in Supplementary Fig. 2. The probe DNA was amplified by PCR.

Antibodies. Antibodies used for immnofluorescence, ChIP and western blotting are as follows: anti-JHDM2A[5], anti-JHDM2B (rabbit polyclonal antibody raised against amino acids 165–465 of human JHDM2B), anti-H3K9me1 (Abcam, ab9045), anti-H3K9me2 (Upstate, 07-441), anti-H3K9me3 (Abcam, ab8898), anti-H3K4me3 (Abcam, ab8580), anti-acH4 (Upstate, 06-866), anti-β-Gal (MPBiologicals, 55976), anti-DNMT3B (a gift from E. Li), anti-γ-H2AX (Abcam, ab22551), anti-5′ methylcytosine (Eutogentec, BI-MECY) and anti-RNA polymerase II (clone H14) (Covance, MMS-134R).

Histology, immunostaining, β-galactosidase and acridine orange staining. For β-galactosidase staining, tissues were fixed with 0.2% glutaraldehyde, 2% formaldehyde, 5 mM EGTA and 2 mM $MgCl_2$ in 0.1 M phosphate buffer (pH 7.3) for 20 min. After rinsing with 0.1% sodium deoxycholate, 0.2% NP-40 and 2 mM $MgCl_2$ in 0.1 M phosphate buffer (pH 7.3), they are stained with 1 mg ml^{-1} X-gal, 5 mM potassium ferricyanide and 5 mM potassium ferrocyanide in rinsing buffer at 37 °C for 4 h to overnight (~12 h). Acridine orange staining was performed as previously described[8].

Electron microscopy. Dissected testes were fixed with 2% paraformaldehyde and 2.5% glutaraldehyde in 0.15 M sodium phosphate buffer (pH 7.4) and transferred onto Epon. Ultrathin sections were stained with both uranyl acetate and lead citrate, and examined with an electron microscope (LEO EM910).

ChIP and ChIP/qPCR. Selected fractions were pooled for specific developmental stages and their purity was further verified by RT–PCR using stage-specific marker genes including *Sycp2* (pachytene spermatocytes), *Brd2* (round spermatids), *Prm2* (round and elongated spermatids), *Aqp8* (elongated spermatids) and *Actb* (housekeeping functions) (Supplementary Fig. 6).

Flow cytometry and sperm-motility analysis. Single-cell preparation and propidium-iodide staining were performed as previously described[9]. The motility of sperm isolated from cauda epididymis was measured by Mutant Mouse Regional Resource Centre at University of North Caroline using Computer Assistant Semen Analysis System (IVOS, Homilton-Thorne Research).

Hormone measurement. Follicle-stimulating hormone, leutinizing hormone, oestradiol, testosterone and androstenedione levels in mouse serum were examined by the Ligand Core Laboratory at University of Virginia.